Journal of the Arkansas Academy of Science

Volume 67 Article 18

2013

Wave Profile for Current Bearing Antiforce Waves

H. Morris
Arkansas Tech University, hmorris3@atu.edu

W. Childs
Arkansas Tech University

P. Pinkston
Arkansas Tech University

M. Hemmati
Arkansas Tech University, mhemmati@atu.edu

J. Christensen
Arkansas Tech University

Wave Profile for Current Bearing Antiforce Waves

H. Morris*, W. Childs, P. Pinkston, M. Hemmati*, and J. Christensen

Arkansas Tech University, Department of Physical Sciences, Russellville, Arkansas 72801, USA

*Correspondence: mhemmati@atu.edu and hmorris3@atu.edu

Running Title: Wave Profile for Current Bearing Antiforce Waves

Abstract

For fluid dynamical analysis of breakdown waves, we employ a one-dimensional, three-component (electrons, ions and neutral particles) fluid model to describe a steady-state, ionizing wave propagating counter to strong electric fields. The electron gas temperature and therefore the electron fluid pressure is assumed to be large enough to sustain the wave motion down the discharge tube. Such waves are referred to as antiforce waves. The complete set of equations describing such waves consists of the equations of conservation of mass, momentum and energy coupled with Poisson's equation.

Inclusion of current behind the wave front alters the set of electron fluid dynamical equations and also the boundary condition on electron temperature. For a range of experimentally observed current values, using the modified boundary condition on electron temperature, we have been able to integrate our modified set of electron fluid dynamical equations through the Debye layer. Our solutions meet the expected boundary conditions at the trailing edge of the wave. We present the wave profile for electric field, electron velocity, electron number density and electron temperature within the Debye layer of the wave.

Introduction

Paxton and Fowler (1962) first presented a one-dimensional, three-component (electrons, ions, and neutral particles), steady-state fluid model with a shock front propelled by electron gas partial pressure. They considered two ionization processes: photoionization and electron impact ionization. Their approximate solution was not completely successful. Loeb (1965), while studying corona discharges, concluded that a wave moves forward due to the cyclic process of photons ionizing and exciting atoms which release photons that continue the process, otherwise known as photo ionization. The emitted radiation has been shown to have no Doppler shift and therefore negligible mass motion. The large difference between the velocities of the positive ions and the electrons due to the electric field force results in creation of a space charge and therefore a space charge field. The electric field accelerates the electrons until they reach a speed sufficient for ionization through collision. This electric field is strongest at the wave front, and in the case of antiforce waves, relative to a reference frame attached to the wave front the electric field force on the electrons propels them in the negative x-direction. However, electron gas pressure is sufficient to sustain wave motion in the positive x-direction. By convention, when the direction of the electric field force is opposite to the direction of wave propagation the wave is referred to as an antiforce wave. For proforce waves, the electric field force and wave propagation share the same direction. Paxton and Fowler (1962) provide the spatial distribution of electric field in the region in front of the breakdown wave and in the transition region of the wave front for a point-plane geometry.

There are two main regions of a wave. The Debye sheath is a thin section occurring behind the shock front where the electric field is at its maximum. At the end of the Debye Sheath the electric field falls to a negligible value and the electron velocity approaches that of heavy particles and ions. After the Debye sheath is the quasi-neutral region. In this thicker, thermal region the electron gas temperature reduces by further ionization, and the ion and electron densities become equal.

Model

Shelton and Fowler (1968) mathematically modeled the proforce wave with no current behind the shock front. There was room for improvement in this model. Fowler et al. (1984) examined various approximations for the proforce case in order to eliminate any discrepancies between theoretical values and experimental results. They determined the

necessity to include a heat conduction term in the energy equation and to accept a discontinuity in the temperature derivative at the shock front. The conservation of energy equation was altered further by taking into consideration the loss of energy electrons experience due to elastic collisions with heavy particles. They employ the zero current condition, $e(N_iV - nv) = 0$, meaning there is no current ahead of the wave. The conservation of mass, momentum, and energy coupled with Poisson's equations for proforce waves they developed are,

$$\frac{d(nv)}{dx} = n\beta, \tag{1}$$

$$\frac{d}{dx}[mnv(v-V) + nkT_e] = -enE - Kmn(v-V), \tag{2}$$

$$\frac{d}{dx}[mnv(v-V)^2 + nkT_e(5v-2V) + 2envΦ - \frac{5nk^2T_e}{mK}\frac{dT_e}{dx}] = -3\left(\frac{m}{M}\right)nkKT_e - \left(\frac{m}{M}\right)Kmn(v-V)^2, \tag{3}$$

$$\frac{dE}{dx} = \frac{e}{\varepsilon_0}(N_i - n), \tag{4}$$

where E, x, β, K, V, M, E_0, k and Φ are the electric field, position in the wave profile, ionization frequency, elastic collision frequency, wave velocity, neutral particle mass, electric field at the wave front, Boltzmann's constant and ionization potential respectively. Also n, v, e, m and T_e are electron concentration, velocity, charge, mass and temperature respectively. N_i is the ion number density in the sheath region. In order to achieve a set of nondimensional equations, the following dimensionless variables were applied:

$$\omega = \frac{2m}{M}, \quad \kappa = \frac{mVK}{eE_0}, \quad \mu = \frac{\beta}{K},$$
$$\alpha = \frac{2e\phi}{mV^2}, \quad \psi = \frac{v}{V}, \quad v = \frac{2e\phi n}{\epsilon_0 E_0^2},$$
$$\theta = \frac{T_e k}{2e\phi}, \quad \eta = \frac{E}{E_0}, \quad \xi = \frac{xeE_0}{mV^2},$$

where ν, ψ, θ, μ, κ, η and ξ are the dimensionless electron concentration, electron velocity, electron temperature, ionization rate, wave constant, electric field, and position inside the wave, respectively. Applying these dimensionless variables results in the nondimensional set of equations for proforce waves:

$$\frac{d}{d\xi}[v\psi] = \kappa\mu v, \tag{5}$$

$$\frac{d}{d\xi}[v\psi(\psi-1) + \alpha v\theta] = -v\eta - \kappa v(\psi-1), \tag{6}$$

$$\frac{d}{d\xi}\left[v\psi(\psi-1)^2 + v\alpha\theta(5\psi-2) + v\psi\alpha + \alpha\eta^2 - \frac{5\alpha^2 v\theta}{\kappa}\frac{d\theta}{d\xi}\right] = -\omega\kappa v[3\alpha\theta + (\psi-1)^2] \tag{7}$$

$$\frac{d\eta}{d\xi} = \frac{v}{\alpha}(\psi-1). \tag{8}$$

Hemmati (1999) derived a set of equations to describe the antiforce case. Previously, Sanmann & Fowler (1975) approximated solutions for antiforce waves with a weak discontinuity at the wave front. To obtain a set of equations for antiforce waves he altered the sign of the constants κ and μ. However, Hemmati's approach entailed a shock at the wave front, and revealed that Sanmann's changes to the dimensionless variables in order to describe the antiforce case were invalid. Hemmati's (1999) non-dimensional variables for antiforce equations are

$$\omega = \frac{2m}{M}, \quad \kappa = -\frac{mVK}{eE_0}, \quad \mu = \frac{\beta}{K},$$
$$\alpha = \frac{2e\phi}{mV^2}, \quad \psi = \frac{v}{V}, \quad v = \frac{2e\phi n}{\epsilon_0 E_0^2},$$
$$\theta = \frac{T_e k}{2e\phi}, \quad \eta = \frac{E}{E_0}, \quad \xi = -\frac{xeE_0}{mV^2},$$

where ν, ψ, θ, μ, κ, η and ξ are the dimensionless electron concentration, electron velocity, electron temperature, ionization rate, wave constant, electric field, and position inside the wave, respectively. After applying these non-dimensional variables, Hemmati's (1999) non-dimensional set of equations for antiforce waves are

$$\frac{d}{d\xi}[v\psi] = \kappa\mu v, \tag{9}$$

$$\frac{d}{d\xi}[v\psi(\psi-1)+\alpha v\theta]=v\eta-\kappa v(\psi-1) \tag{10}$$

$$\frac{d}{d\xi}[v\psi(\psi-1)^2+\alpha v\theta(5\psi-2)+\alpha v\psi+\alpha\eta^2-\frac{5\alpha^2 v\theta}{\kappa}\frac{d\theta}{d\xi}]=-\omega\kappa v[3\alpha\theta+(\psi-1)^2] \tag{11}$$

$$\frac{d\eta}{d\xi}=-\frac{v}{\alpha}(\psi-1). \tag{12}$$

These equations were integrated through the sheath region and the resultant plots show that the solutions meet the expected conditions at the trailing edge of the wave.

Hemmati et al. (2011) further investigated antiforce waves with large current behind the wave front. To meet this condition, the current behind the wave front is taken to be $I_1 = eN_iV_i - env$, where N_i and V_i are ion number density and velocity within the sheath. No Doppler shift has been observed during these phenomena showing negligible neutral particle and ion motion in the laboratory frame. Therefore, V_i and V are assumed to be approximately equivalent. Solving for N_i, substituting the resultant expression into equation (4), and employing the nondimensional variables for antiforce waves results in the following equation:

$$\frac{d\eta}{d\xi}=\frac{\kappa I_1}{\varepsilon_0 KE_0}-\frac{v}{\alpha}(\psi-1). \tag{13}$$

Defining ι as $\frac{I_1}{\varepsilon_0 KE_0}$ and substituting into the previous equation leads to Poisson's equation for antiforce waves with current behind the wave front.

$$\frac{d\eta}{d\xi}=\kappa\iota-\frac{v}{\alpha}(\psi-1). \tag{14}$$

Substituting the previous equation into the antiforce equation for conservation of energy (11), results in a complete set of electron fluid-dynamical equations for current bearing antiforce waves. All quantities are assumed intrinsically positive, including κ. The complete set of equations become

$$\frac{d}{d\xi}[v\psi]=\kappa\mu v, \tag{15}$$

$$\frac{d}{d\xi}[v\psi(\psi-1)+\alpha v\theta]=v\eta-\kappa v(\psi-1) \tag{16}$$

$$\frac{d}{d\xi}\left[v\psi(\psi-1)^2+\alpha v\theta(5\psi-2)+\alpha v\psi+\alpha\eta^2-\frac{5\alpha^2 v\theta}{\kappa}\frac{d\theta}{d\xi}\right]=2\eta\kappa\iota\alpha-\omega\kappa v[3\alpha\theta+(\psi-1)^2], \tag{17}$$

$$\frac{d\eta}{d\xi}=\kappa\iota-\frac{v}{\alpha}(\psi-1). \tag{18}$$

Results and Discussion

Rakov's (2000) study of positive and bipolar lightning yielded wave speed values between $0.3\text{x}10^8$ – $1.7\text{x}10^8$ m/s. While studying the direct measurement of the time derivative of the electric field for triggered lightning strokes, Uman et al. (2000) measured return stroke speeds as low as $0.46\text{x}10^8$ m/s. Idone's et al. (1987) research yielded wave speed values between $0.9\text{x}10^8$ – $1.6\text{x}10^8$ m/s.

Rakov (2000), in his review of characteristics of positive and bipolar lightning reported a return stroke current of 10 kA. Wang et al. (1999), while studying rocket triggered lightning strokes, reported a current peak value around 12 to 21 kA. Uman et al. (2000), while investigating the time derivative of the electric field 10, 14, and 30 m away from triggered lightning strokes, observed peak current values for return strokes up to 30.4 kA. The dimensionless current value of ι = 1 represents a current value of approximately 10 kA.

A trial and error method of integration was employed to attain solutions to eqs. (15-18). For α = 0.001, or wave speed value of $9.37\text{x}10^7$ m/s, values at the wave front for the wave constant, κ, electron number density, ν_1, and electron velocity, ψ_1, were chosen. If these values did not satisfy the boundary conditions at the end of the sheath region, they were modified. The values of κ, ν_1 and ψ_1 were repeatedly altered until the solutions met the boundary conditions at the end of the sheath ($\psi \to 1$ and $\eta \to 0$). For dimensionless current values of 0.1, 0.25, 1.5, 2.6, 7 and 15, solutions were found for α = 0.001 or wave speed value of $9.37\text{x}10^7$ m/s. The following initial variable values result in successful solutions to the electron fluid-dynamical equations (15-18).

$$\iota = 0.1,\ \kappa = 0.144,\ \psi_1 = 0.5219,\ \nu_1 = 0.1735$$

ι= 0.25, κ= 0.144, ψ_1= 0.5202, ν_1= 0.1765

ι = 1.5, κ= 1.44, ψ_1= 0.513, ν_1= 0.1855

ι = 2.6, κ= 1.44, ψ_1= 0.5049, ν_1= 0.1879

ι = 7, κ= 0.144, ψ_1= 0.4721, ν_1= 0.2161

ι = 15, κ= 0.144, ψ_1= 0.409, ν_1= 0.2406

For antiforce waves with a significant current behind the shock front, Figure 1 represents dimensionless electric field, η, as a function of dimensionless electron velocity, ψ, within the sheath region of the wave for dimensionless current values of 0.1, 0.25, 1.5, 2.6, 7, and 15 at a wave velocity of 9.37×10^7 m/s. All current values except for ι = 15 satisfy the boundary conditions at the end of the sheath region; that is, η approaches zero as nondimensional electron velocity, ψ, approaches 1.

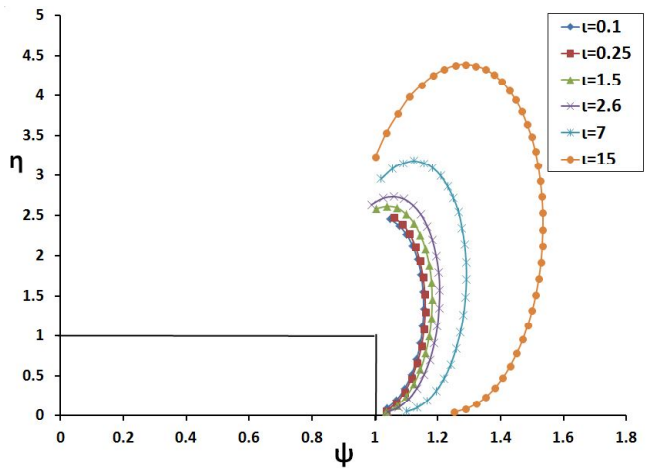

Figure 1. Electric field, η, as a function of electron velocity, ψ, within the sheath region of current bearing antiforce waves for a wave speed value of α=0.001 and for current values 0.1, 0.25, 1.5, 2.6, 7 and 15.

Upon closer inspection of the curve with a dimensionless current value of 15 in Fig. 1, one can see that it does not meet the boundary condition ($\psi \rightarrow 1$) at the end of the sheath region. Hence, ι = 7 seems to be the cut off point for which valid solutions were found.

For antiforce waves with a large current behind the shock front, Figure 2 shows dimensionless electric field, η, as a function of dimensionless position within the sheath region, ξ, for all previously listed current values.

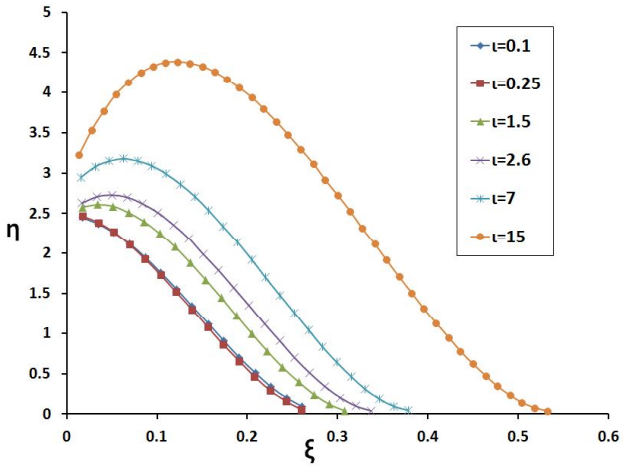

Figure 2. Electric field, η, as a function of position, ξ, within the sheath region of current bearing antiforce waves for a wave speed value of α=0.001 and for current values 0.1, 0.25, 1.5, 2.6, 7 and 15.

Our results indicate that the sheath thickness is dependent upon the magnitude of current behind the wave front. For a dimensionless current value of 15, the largest current value examined, the dimensionless position within the sheath, ξ, is 0.54. This translates into a sheath thickness of 0.27 cm. When considering the dimensionless current value of 0.1, the smallest current value examined, the dimensionless position within the sheath, ξ, is 0.28. This value translates into a sheath thickness of 0.13 cm. Previous works have shown that as wave velocity increases the sheath thickness becomes smaller and smaller. Our wave velocity of 9.37×10^7 m/s is a relatively fast wave speed. Fujita et al. (2003) while measuring electron density behind shock waves determined a sheath thickness of 5 cm. For α = 0.01 and a wave velocity of 3×10^7 m/s, Hemmati (2011), while studying current bearing antiforce waves, reported a sheath thickness of 2.5 cm.

For antiforce waves with a significant current behind the shock front, Figure 3 represents dimensionless electron velocity, ψ, as a function of dimensionless position within the sheath region, ξ, for all aforementioned current values.

For antiforce waves with a large current behind the shock front, Figure 4 represents dimensionless electron number density, ν, as a function of dimensionless position, ξ, within the sheath region for all above mentioned current values. Taking the dimensionless average electron number density from this plot, ν = 0.09, we can calculate our average electron number density to be 9.95×10^{18} m^{-3}. While modeling micro-discharges in plasma utilizing a two-dimensional fluid

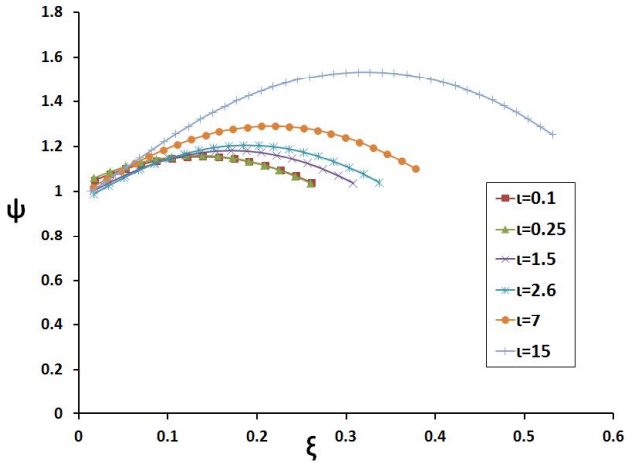

Figure 3. Electron velocity, ψ, as a function of position, ξ, within the sheath region of current bearing antiforce waves for a wave speed value of α=0.001 and for current values 0.1, 0.25, 1.5, 2.6, 7 and 15.

model, Hagelaar and Kroesen (2000) reported an electron number density of 10^{18} m^{-3}. Jurenka and Barreto (1985), while studying electron waves in the electrical breakdown of gases with application to the dart leader in lightning, reported electron number density values around 10^{21} – 10^{23} m^{-3}. Fujita et al. (2003) reported an electron number density of 10^{22} m^{-3} while studying electron number density behind shock waves.

For antiforce waves with a large current behind the shock front, Figure 5 represents dimensionless electron temperature, θ, as a function of dimensionless position, ξ, within the sheath region for all aforementioned current values. Our dimensionless electron temperature value of θ = 250 corresponds to an electron gas temperature of $1.16x10^{7}$ K. While studying ionizing waves propagating counter to strong electric fields, Sanmann and Fowler (1975) observed that the electron temperature increases very rapidly away from the wave front until it reaches a peak value around $3.17x10^{7}$ K. Hemmati et al. (2011), while studying antiforce waves with a large current behind the wave front, determined an electron temperature of $3.88x10^{7}$ K.

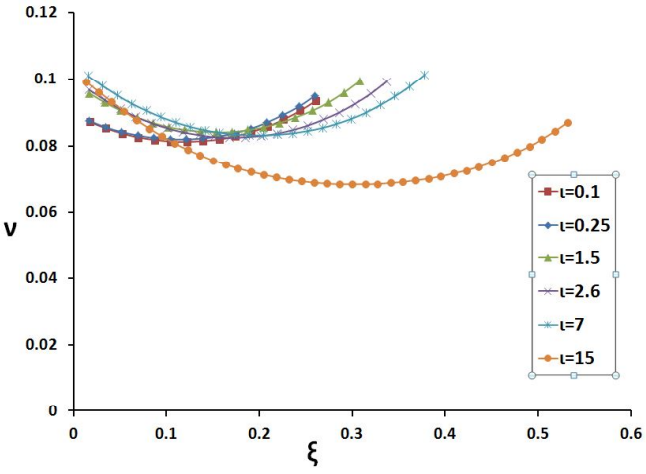

Figure 4. Electron number density, ν, as a function of position, ξ, within the sheath region of current bearing antiforce waves for a wave speed of α=0.001 and for current values 0.1, 0.25, 1.5, 2.6, 7 and 15.

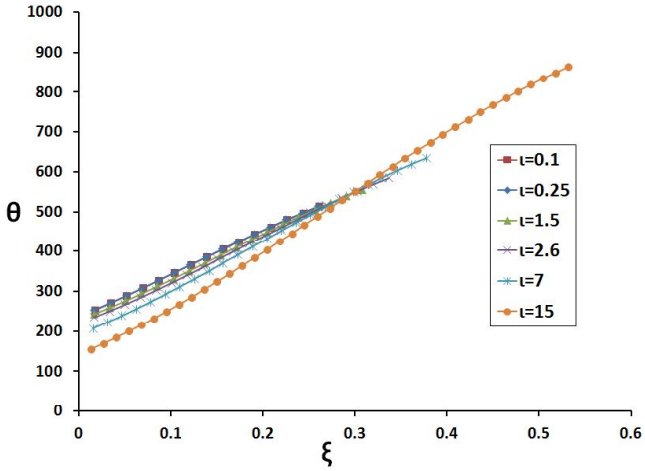

Figure 5. Electron temperature, θ, as a function of position, ξ, within the sheath region of current bearing antiforce waves for a wave speed of α=0.001 and for current values 0.1, 0.25, 1.5, 2.6, 7 and 15.

Conclusions

Solutions to the modified set of electron fluid-dynamical equations for antiforce waves bearing significant current behind the wave front were found that satisfied the boundary conditions at the end of the sheath for dimensionless current values of 0.1, 0.25, 1.5, 2.6, and 7. It seems the dimensionless current value ι = 7 is the cut off point for which integration of the set of electron fluid dynamical equations through the dynamical transition region becomes possible. Our results are in good agreement with other experimental works.

Acknowledgements

The authors would like to express gratitude to the Arkansas Space Grant Consortium for the financial support of this research.

Literature Cited

Fowler RG, **M Hemmati**, **RP Scott** and **S Parsendajadh**. 1984. Electric breakdown waves: Exact numerical solutions. Part 1. The Physics of Fluids 27(6):1521-1526.

Fujita K, **S Sato** and **T Abe**. 2003. Electron density measurements behind shock waves by H-β profile matching. Journal of Thermodynamics and Heat Transfer 17:210-6.

Hagelaar GJM and **GMW Kroesen**. 2000. Modeling of the microdischarges in plasma addressed liquid crystal displays. Journal of Applied Physics 88(5):2252-2262.

Hemmati M. 1999. Electron Shock Waves: Speed Range for Antiforce Waves. Proceedings. of 22nd International Symposium on Shock Waves. Pp. 995-1000.

Hemmati M, **W Childs**, **H Shojaei** and **D Waters**. 2011. Antiforce Current Bearing Waves. Proceedings of 28th International Symposium on Shock Waves.

Idone VP, **RE Orville**, **DM Mach** and **WD Rust**. 1987. The propagation speed of a positive lightning return stroke. Geophysical Research Letters 14(11):1150-1153.

Jurenka H and **E Barreto**. 1985. Electron waves in the electrical breakdown of gases with application to the dart leader in lightning. Journal of Geophysical Research 90(D4):6219-6224.

Loeb LB. 1965. Ionizing waves of potential gradient. Science 148(3676):1417.

Paxton GW and **RG Fowler**. 1962. Theory of breakdown wave propagation. Physics Review. 128(3):993-997.

Rakov VA. 2000. Positive and Bipolar Lightning Discharges: A Review. Proceedings of 25th International Conference on Lightning Protection. p 103-108.

Sanmann E and **RG Fowler**. 1975. Structure of electron fluid dynamical plane waves: Antiforce waves. The Physics of Fluids 18(11):1433-1438.

Shelton GA and **RG Fowler**. 1968. Nature of Electron-Fluid Dynamical Waves. The Physics of Fluids 11(4):740-746.

Uman MA, **VA Rakov**, **KJ Schnetzer**, **JK Rambo**, **DE Crawford** and **RJ Fisher**. 2000. Time derivative of the electric field 10, 14, and 30 m from triggered lighting strokes. Journal of Geophysical Research 105(D12):15,577-15,595.

Wang D, **VA Rakov**, **MA Uman**, **N Takagi**, **T Watanabe**, **DE Crawford**, **KJ Rambo**, ***et al***. 1999. Attachment process in rocket-triggered lightning strokes. Journal of Geophysical Research 104(D2):2143-50.